RGNZ/MGPB

Subsidence prediction for twin tunnels using Genetic algorithms-case study: Isfahan, Iran

Rudarsko-geološko-naftni zbornik
(The Mining-Geology-Petroleum Engineering Bulletin)
DOI: 10.17794/rgn.2025.4.5

Preliminary communication

Amirhossein Rostami[1]*, Hamid Chakeri[2], Kurosh Shahriar[3], Masoud Cheraghi Seifabad[4]

[1] *Department of Mining Engineering, South Tehran Branch, Islamic Azad University, Tehran, Iran.*
[2] *Department of Mining Engineering, Sahand University of Technology, Tabriz, Iran.*
[3] *Department of Mining and Metallurgy Engineering, Amir Kabir University of Technology, Tehran, Iran.*
[4] *Department of Mining Engineering, Isfahan University of Technology, Isfahan, Iran.*

Abstract

Today, with the increasing pace of urbanization and population growth, the demand for metro tunnels has risen significantly. These tunnels are often constructed at shallow depths and in close proximity to urban infrastructure. In such scenarios, it becomes crucial to safeguard buildings and other structures from potential damage caused by metro tunnel excavation. Therefore, studying ground movements and surface settlements induced by these tunnels is essential to ensure the safety of surface structures. In this research, based on the geotechnical conditions of the study area and data collected during the excavation of twin metro tunnels using a Tunnel Boring Machine (TBM), an empirical method was developed to estimate subsidence, maximum subsidence, and inflection points. Boltzmann and Gaussian functions were employed to derive these parameters. Furthermore, a sensitivity analysis was conducted using three-dimensional Plaxis software for the cross-section of Si-o-se-pol alongside three other soil types. A numerical relationship for predicting maximum subsidence was then proposed using a genetic algorithm. The results revealed strong alignment between the empirical and numerical approaches derived in this study. Consequently, these findings enable the accurate prediction of ground subsidence for Isfahan Metro Line 2, which is now under excavation.

Keywords:
subsidence, maximum subsidence, inflection point, empirical formula, numerical formula

1. Introduction

In urban tunnelling projects, assessing the subsidence level is a crucial parameter. Researchers have proposed various approaches to calculating and estimating subsidence, which can be broadly classified into empirical, analytical, and numerical methods.

Empirical methods primarily rely on field data and the correlation of various parameters, including geological conditions. However, one of their significant limitations lies in their specificity, as they are developed for particular geological settings. Therefore, careful consideration is essential when applying them to different conditions.

Among the various empirical methods, the Litwinnisym method (1956) is noteworthy (**Chakeri et al., 2013**). This method assumes that the constituent components of soil layers can be represented as numerous spheres of uniform size in three dimensions or as two-dimensional discs. These elements were incorporated into the proposed model. In 1969, **Peck**, drawing on extensive data from numerous tunnelling projects, applied a Gaussian curve to estimate the subsidence at the surface directly above tunnels. Later, in **1979, Oteo** developed an experimental approach by refining Peck's method, incorporating several parameters to account for the geomechanical conditions of excavation sites. Similarly, **Oreili & Neo (1982)** introduced two separate methods tailored for sticky and granular soils in the United Kingdom based on their observations. In recent years, researchers have offered various methodologies to address subsidence. Notable contributions include **Attewell et al. (1982)** on three-dimensional subsidence profiles, **Herzog (1985)** on assessing settlement for single and twin tunnels, and **Schmidt (1969) and Arioglu's (1992)** work on the maximum subsidence associated with single tunnels. Additionally, **Mair et al. (1993)** developed a method to estimate subsidence levels and measure inflection points. **Chakeri et al. (2013)** utilized numerical modelling and data analysis from three metro tunnels located in Mashhad, Tehran, and Istanbul. Their research provided insight for predicting maximum subsidence

* Corresponding author: Amirhossien Rostami
e-mail address: arostami80@gmail.com
Received: 10 November 2024. Accepted: 25 February 2025.
Available online: 27 August 2025

during mechanized tunnelling processes. Analytical methods derived from solving equations have also been widely used to address varying geological conditions. One such example is **Verruijt & Booker's (1996)** method, which builds upon **Sagasta's (1987)** work to describe tunnel deformation through radial contraction and elliptical deformation. The **Loganathan & Polos (1998)** method further refined this approach by introducing calculations for subsidence based on the gap parameter, as first referenced by **Lee et al. (2001). Gonzales & Sagasta (2001)** also contributed to this area by expanding on this methodology with additional empirical insight into subsidence phenomena.

Numerical modelling has been extensively employed in various tunnelling studies to analyze and predict ground behaviour and associated impacts. For instance, **Najjar & Zaman (1993)** developed a nonlinear finite-element analysis method aimed at predicting surface subsidence caused by underground construction. Their study incorporated complex soil behaviour models that accounted for material nonlinearity and time-dependent effects, resulting in more accurate and reliable predictions compared to conventional linear methods. These advancements provided deeper insight into surface movements resulting from subsurface operations. **Selby (1999)** examined the effects of tunnelling-induced ground movements on buildings in Workington, UK, with a particular emphasis on soil deformation and its connection to tunnel design and ground conditions. The research highlighted strategies to mitigate surface settlement and minimize structural damage, offering crucial recommendations for urban tunnelling practices. **Wang et al. (2000)** focused on developing predictive tools to estimate surface settlements in soft ground conditions. By comparing empirical, analytical, and numerical approaches, their study evaluated the accuracy of each method in predicting settlement profiles across diverse geotechnical scenarios. These models play a significant role in improving the precision and reliability of settlement forecasting for better tunnelling project management. **Das et al. (2017)** utilized finite element modelling to explore surface subsidence caused by asymmetrically aligned parallel highway tunnels. The research investigated the impact of factors such as tunnel spacing, alignment, and geological conditions on settlement patterns. Their findings offered actionable insight for designing safer and more efficient tunnel structures, especially in challenging geotechnical environments. **Chen et al. (2016)** conducted a numerical analysis of surface settlements arising from double-O tube shield tunnelling. The study assessed how factors such as soil properties, tunnel depth, and construction techniques influence settlement behaviour. The results provided valuable guidance for mitigating ground deformation and ensuring the safety of surrounding infrastructure during construction. Finally, **Kim (1996)**, in their doctoral dissertation at the University of Oxford, addressed the interactions between tunnels in clay using model testing and analytical methods. The research delved into the effects of tunnel spacing, soil properties, and construction sequences on ground deformation and stress distribution. These findings offered a deeper understanding of tunnel behaviour in cohesive soils, contributing to enhanced design strategies for underground infrastructure.

Chapman et. al (2007) explore ground movements resulting from the construction of multiple tunnels in soft soils through laboratory model tests. Their research assesses the effects of tunnel geometry, construction sequence, and spacing on settlement and soil deformation patterns. The study enhances the understanding and forecasting of ground behaviour in multi-tunnel projects set in soft ground conditions. Similarly, **He el al. (2012)** focus on surface settlement caused by twin-parallel shield tunnelling in sandy cobble formations. Using field monitoring and numerical modelling, they analyze how factors such as soil properties, tunnel depth, and spacing influence settlement patterns. Their findings offer practical insight for minimizing settlement risks in complex geological environments during shield tunnelling operations. **Fang el al. (2015)** propose a predictive model for surface settlement by integrating shield tunnel driving tests with analytical methods. By combining experimental data from model tests with theoretical approaches, they provide a robust framework for understanding the settlement process, aiding in more accurate predictions and improved tunnel design across diverse ground conditions.

Fang el al. (2017) investigate surface settlement resulting from Earth Pressure Balance (EPB) shield tunnelling in sandy soils. Their research introduces a predictive model that combines empirical and numerical approaches to evaluate the influence of tunnelling parameters, soil characteristics, and tunnel design on surface deformation. The study's outcomes seek to refine the precision of settlement predictions and promote safer tunnelling practices in sandy environments.

Wang et al. (2022) introduced an innovative method for calculating stratum settlement resulting from tunnelling activities. This approach incorporates the effects of tunnel construction processes and varying ground conditions on settlement behaviour. By enhancing the precision of settlement predictions, the method offers a more dependable tool for tunnel design and risk evaluation across diverse geotechnical settings. In a separate study, **Ahmed et al. (2023)** performed a numerical analysis of surface movements caused by tunnelling, with a specific focus on MRT Line 1 in Dhaka. Through numerical modelling, the research examined how tunnelling impacts surface settlement and nearby infrastructure, accounting for factors such as soil conditions and tunnel depth. The findings offer crucial insight to help mitigate ground movement challenges associated with tunnels in urban environments.

Alsirawan et al. (2023) introduce a two-dimensional numerical modelling approach to examine structure set-

Table 1. Summary of Research Methods

<table>
<tr><th colspan="4">Research method</th></tr>
<tr><th colspan="3">Collecting behavioural data</th><th>Collecting geomechanical information for four soil types</th></tr>
<tr><td rowspan="2">Presenting the Subsidence Curve with Excel Software</td><td colspan="2">Presenting the Subsidence curve with OriginLab software with two Boltzmann and Gaussian functions</td><td>Numerical analysis of four soil types with Plaxis 3D software</td></tr>
<tr><td>Determining the Subsidence rate, maximum Subsidence, and inflection point with the Gaussian function</td><td>Determining the Subsidence rate, maximum Subsidence, and inflection point with the Boltzmann function</td><td>Data analysis of Plaxis 3D software with Genetic algorithm</td></tr>
<tr><td colspan="3">Presenting an Empirical relationship</td><td>Presenting a Numerical relationship</td></tr>
<tr><td colspan="4">Proper agreement of the Subsidence rate obtained from the numerical relationship with the empirical relationship</td></tr>
</table>

tlement caused by tunnelling with a Tunnel Boring Machine (TBM). Their research includes a parametric analysis to evaluate the influence of factors like soil characteristics, tunnel depth, and construction parameters on settlement behaviour. The study provides practical insight and recommendations to help mitigate settlement effects on structures during TBM tunnelling operations.

Khoshzaher et al. (2023) present a methodology to predict the performance of Earth Pressure Balance (EPB) Tunnel Boring Machines (TBM) by utilizing Firefly Algorithms and Particle Swarm Optimization (PSO). Their research introduces an optimized model that integrates diverse operational parameters and ground conditions, improving the accuracy of TBM performance predictions. The results provide a valuable tool for enhancing tunnelling operations and facilitating informed decision-making in challenging geotechnical settings. **Jaberi & Zare (2023)** examine the influence of various soil parameters and behavioural models on settlement predictions caused by tunnelling, using the Qom Metro Line A as a case study. The investigation evaluates the reliability of different soil models in simulating surface settlement under varying ground conditions. The outcomes underscore the critical role of selecting suitable soil behaviour models to achieve precise settlement predictions and effectively manage risks in urban tunnelling ventures. **Krishna & Maji (2023)** focus on tunnelling-induced ground settlements with an emphasis on soil variability. In addition to surface settlement, numerical modelling was utilized for analyzing deformation distributions around tunnels (e.g. **Unlu & Gercek, 2003**; **Vlachopoulos & Diederichs, 2009**; **Basarir et al., 2010**; **Sakcali and Yavuz, 2019**) and for TBM-based tunnelling studies (e.g. **Zhao et al., 2017**; **Hasanpour et al., 2014**; **Sakcali & Yavuz, 2022**). Their proposed model incorporates variations in soil properties to deliver more accurate settlement predictions. The findings highlight the importance of addressing soil heterogeneity to ensure reliable settlement forecasts and safeguard the stability of nearby infrastructure during tunnelling activities.

Despite numerous studies on surface settlements caused by tunnelling, most available methods are limited by specific geological conditions or fail to comprehensively integrate empirical, analytical, and numerical approaches. This study aims to bridge that gap by combining empirical formulas, numerical modelling, and genetic algorithms to predict ground subsidence caused by twin tunnel excavations. The objective of this research is to develop a reliable and accurate prediction model for surface settlement in varying soil conditions using data from Isfahan Metro Line 2 as a case study. By doing so, we seek to enhance the safety and efficiency of tunnelling projects in complex urban environments.

This study focuses on measuring the extent of ground subsidence caused by the excavation of a metro tunnel using a TBM, based on monitoring data. Through data analysis, a method has been developed to determine the maximum subsidence and the corresponding inflection point. A summary of the research activities is presented in **Table 1**.

2. Materials and Methods

2.1. The Suggested Equations

The empirical approach relies on formulas derived from past observations combined with certain field measurements. Various methods have been proposed, grounded in field data, for predicting surface settlement, as summarized in **Table 2**.

2.2. Genetic algorithms (GA)

Genetic algorithms, or GAs, are optimization tools inspired by natural selection and evolutionary principles. They begin by creating an initial set of candidate solutions, which are then refined over successive generations through selection, crossover, and mutation processes. This iterative approach continues until an optimal or near-optimal solution is achieved. Thanks to their ability to handle complex and nonlinear parameter interactions, GAs are particularly well-suited for tackling challenges in geotechnical engineering.

In recent years, significant research has focused on the application of genetic algorithms (GAs) in geotech-

Table 2. Empirical formulas for estimating surface settlement values

Researcher(s)	Empirical solution	Explanation
Litwinnisym (1956)	$\delta_{V(Y\text{-}Z)} = \frac{0.8t}{K_a}\left(\frac{Z_0 - Z}{2a}\right)^{-n} EXP\left[-0.5\left(\frac{y}{a\,k_a}\right)^2\left(\frac{Z_0 - Z}{2a}\right)^{-2n}\right]$ $\delta_{v_{max}} = \frac{0.8t}{a}\left(\frac{Z}{D}\right)^{-n} \quad V_s = Dt; \quad S_{V.max} = \frac{0.8V_s}{DK_a}\left(\frac{Z}{D}\right)^{-n}$	z_0: Depth of tunnel k_a and n: Experimental coefficients D: Tunnel diameter V_s: Volume loss of the soil layer
Peck (1969)	$S_{V(m)} = S_{V(max)} EXP\left(-\frac{y^2}{2i^2}\right)$	S_v: Subsidence at the transverse section of the tunnel $S_{v(max)}$: Maximum subsidence y: Distance to tunnel axis i: Inflection point
Oteo (1979)	$\omega_{(y)} = \varphi\frac{\gamma(2a_0)^2}{E}(0.85 - \vartheta)EXP\left[-\frac{y^2}{2i^2}\right]$ $i = a_0\eta\left(1.05\frac{Z_0}{a_0} - 0.42\right)$	E: Young's modulus a_0: Tunnel radius z_0: Tunnel depth ϑ: Poisson's ratio φ: Internal friction angle i: Inflection point
Oreili & Neo (1982)	$i = 0.43Z + 1.1\left(r^2 = 0.96\right)$ (1) If $3 \le Z \le 34$m $i = 0.28Z - 0.1(r^2 = 0.78)$ (2) If $6 \le Z \le 10$m	Formula 1: For the sticky grounds Formula 2: For the grains grounds
Attewell & Woodman (1982)	$S = \frac{V_s}{i.\sqrt{2\pi}}.EXP\left[-\frac{y^2}{2i^2}\right]\cdot\left\{G\left[\frac{X - X_i}{i}\right] - G\left[\frac{X - X_F}{i}\right]\right\}$ $G = (X - Xi)/i$	S: Surface vertical subsidence at position (x-y) X: Position of the supposed surface of the longitudinal plane Y: Distance of the given point from the axis of the tunnel V_s: Volume of subsidence for the tunnel advance per meter, expressed as a percentage of V_l X_i: Initial position or tunnel cross section X_f: Position of the tunnel advance
Herzog (1985)	$S_{max} = 0.785(\gamma_n Z_0 + \sigma_s)\left(\frac{D^2}{iE}\right)$ (single tunnel) $S_{max} = 4.71(\gamma_n Z_0 + \sigma_s)\left(\frac{D^2}{(3i + a)E}\right)$ (twin tunnels)	γ_n: Soil specific gravity z_0: Depth of the tunnel σ_s: Surface surcharge D: Tunnel diameter i: Inflection point a: Distance between two tunnels E: Young's modules
Schmidt (1969) and Arioglu (1992)	$S_{max} = 0.0125K\left(\frac{R^2}{i}\right)$ $K = 0.87EXP[0.26N] = 0.87EXP\left[0.26\left(\frac{\gamma_n Z_0 + \sigma_s + \sigma_T}{C_U}\right)\right]$	γ_n: Soil specific gravity z_0: Depth of the tunnel σ_s: Surface surcharge σ_T: Face pressure by TBM C_U: Undrained soil adhesion
Chakeri et al. (2014)	$s_{max} = 3198.744\left(\frac{D}{Z_0}\right) * \left(\left(\frac{\gamma Z_0 + \sigma_s - (c + 0.3\sigma_T)}{E}\right)(1 - \vartheta)(1 - \sin\sin\varphi)\right)^{0.8361}$	D: Tunnel diameter γ: Soil specific gravity Z_0: Depth of the tunnel σ_s: Surface surcharge c: Cohesion σ_T: Face pressure by TBM E: Young's modulus ϑ: Poisson's ratio φ: Internal friction angle.

nical engineering. Rooted in the principles of natural selection and genetics, GAs have emerged as a robust stochastic optimization method (**Chakeri et al., 2014; Cui & Sheng, 2005**). This approach has demonstrated its effectiveness in addressing complex combinatorial design challenges within the field (**Andrab et al., 2017**). In particular, employing real-coded GA as an optimization tool has proven valuable for determining soil parameters in geotechnical studies (**Jin et al., 2017**). Furthermore, integrating GAs with numerical analysis software, such as Plaxis, has shown considerable potential in enhancing sensitivity analyses for geotechnical problems (**Vahdati et al., 2014; Benayoun et al., 2020**).

The A and B coefficients in the formula (*) used in this study were optimized for various soil types through genetic algorithms (GA). To implement GA, an initial random population of A and B coefficient values was generated and evaluated based on their ability to match data derived from a sensitivity analysis conducted using the three-dimensional Plaxis program. The best-fitting solutions from this population were selected via crossover and mutation processes, reproduced, and combined to create new candidate solutions. This iterative procedure was repeated across multiple generations, ultimately refining the A and B coefficients to optimized values.

The findings demonstrated that applying GA significantly enhanced the accuracy of the numerical models by improving the A and B coefficients. These optimized coefficients provided a more precise fit to the experimental data, making the numerical models more reliable for designing and analyzing underground structures. This highlights the effectiveness of genetic algorithms as a robust optimization method in geotechnical engineering, adept at addressing complex parameter interdependencies and improving numerical model.

Table 3. Monitoring Data

Row	Distance from TBM (m)	Subsidence (mm)
1	-36	0
2	-24	0
3	-13	-1
4	-1	-2
5	2	-4
6	10	-6
7	20	-7
8	34	-8
9	48	-8
10	62	-8
11	85	-8

2.3. Case study

The North-South metro line in Isfahan represents the primary focus of the Isfahan Metro development, linking the northern Kaveh bus terminal to the southern Soufe bus terminal. The project employed the excavation of twin tunnels utilizing Tunnel Boring Machines (TBM) with a diameter of 6.9 meters. The structural design featured a center-to-center distance of 18.12 meters between the two tunnels, each with an effective diameter of 6.6 meters and lined with 30 cm thick concrete segments. Excavation began with the western tunnel, and geotechnical conditions along the route were assessed based on data collected from boreholes drilled in advance. The geological profile of the area comprises three distinct soil layers, with thicknesses of 6.1 meters, 4.5 meters, and 8.58 meters for the first, second, and third layers respectively. The tunnel alignment traversed through the second and third layers, as identified in prior studies (**Rostami, 2017**).

2.4. Experimental analysis

The application of the Boltzmann function to model particle distribution and the Gaussian function in Geostatistics for identifying intricate patterns in engineering is highly remarkable. This study focused on determining

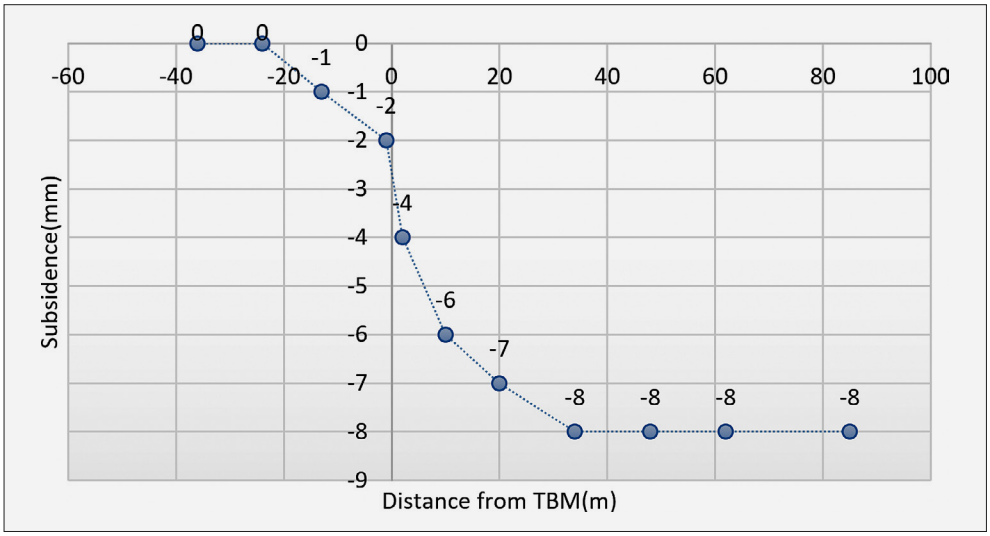

Figure 1. Subsidence monitoring diagram created using Excel software

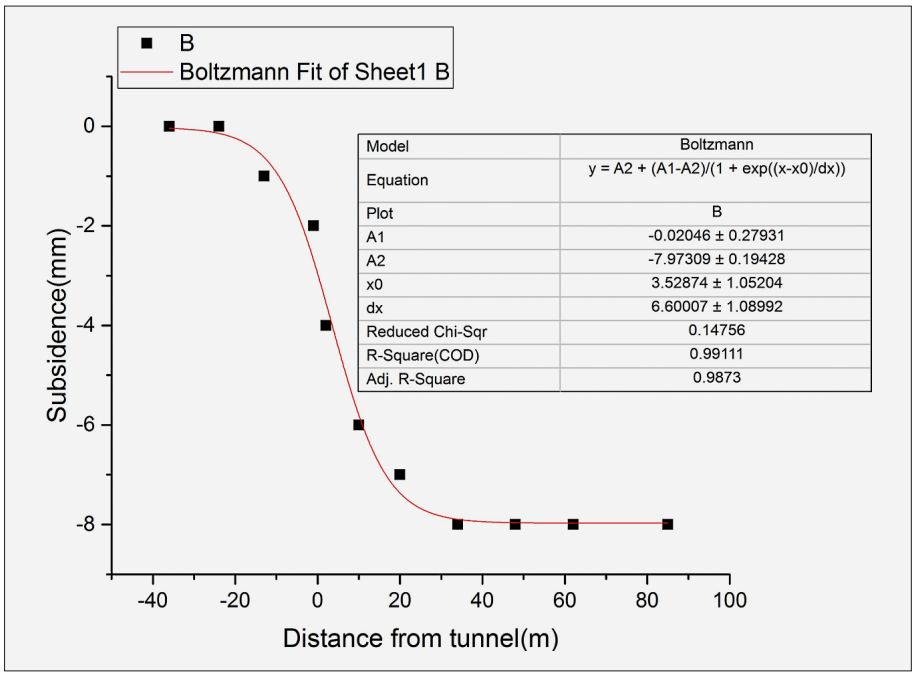

Model	Boltzmann
Equation	y = A2 + (A1-A2)/(1 + exp((x-x0)/dx))
Plot	B
A1	-0.02046 ± 0.27931
A2	-7.97309 ± 0.19428
x0	3.52874 ± 1.05204
dx	6.60007 ± 1.08992
Reduced Chi-Sqr	0.14756
R-Square(COD)	0.99111
Adj. R-Square	0.9873

Figure 2. Subsidence profile represented using a Boltzmann function

the displacement of soil particles through monitoring while utilizing these functions to analyze their distribution. Project monitoring involved the installation of NAK2 cameras, spaced 50 meters apart along the main axis of the tunnel. Additionally, cameras were placed at 100-meter intervals along the eastern, western, and mid-western sidewalks during TBM machine drilling operations. **Table 3** provides an example that illustrates a situation where a camera, positioned 30 meters from the tunnel's front face, recorded subsidence of approximately 8 mm. Using the data from **Table 3**, **Figure 1** was generated with Excel software.

The monitoring data, analyzed using OriginLab software, yields the following empirical formulas for the subsidence of the twin metro tunnels in Isfahan, derived from Boltzmann and Gaussian functions. The Boltzmann function graph, based on the data presented in **Table 3**, is illustrated in **Figure 2**.

An inflection point was formed as a result of the dual impact brought about by the derivative of the formula mentioned earlier.

$$y = A_2 + \frac{(A_1 - A_2)}{\left(1 + e^{\frac{(x-x_0)}{d(x)}}\right)} = A_2 + \frac{k_1}{\left(1 + e^{\frac{(x-x_0)}{d(x)}}\right)}; \; y = \frac{a}{f(x)};$$

$$y' = \frac{-af(x)}{f^2(x)}; \; y' = 0 + \frac{-k_1\left(\frac{1}{dx}e^{\frac{(x-x_0)}{d(x)}}\right)}{\left(1 + e^{\frac{(x-x_0)}{d(x)}}\right)^2};$$

$$h_{(x)} = -k_1\left(\frac{1}{dx}e^{\frac{(x-x_0)}{d(x)}}\right); \; g_{(x)} = \left(1 + e^{\frac{(x-x_0)}{d(x)}}\right)^2;$$

$$y'' = \frac{h'(x)g(x) - h(x)g'(x)}{g^2(x)}$$

$$y'' = \frac{\left(-\frac{k_1}{dx^2}e^{\frac{(x-x_0)}{d(x)}}\right)\left(1 + e^{\frac{(x-x_0)}{d(x)}}\right)^2 + \left(\frac{k_1}{dx}e^{\frac{(x-x_0)}{d(x)}}\right)\left(\frac{2}{dx}e^{\frac{(x-x_0)}{d(x)}}\right)\left(1 + e^{\frac{(x-x_0)}{d(x)}}\right)}{g^2(X)}$$

$$y'' = \frac{\left(\frac{k_1}{dx^2}e^{\frac{(x-x_0)}{d(x)}}\right)\left(1 + e^{\frac{(x-x_0)}{d(x)}}\right)\left[\left(-(1 + e^{\frac{(x-x_0)}{d(x)}})\right) + 2e^{\frac{(x-x_0)}{d(x)}}\right]}{g^2(X)} \cong 0$$

$$s_1 = \left(\frac{k_1}{dx^2}e^{\frac{(x-x_0)}{d(x)}}\right)\left(1 + e^{\frac{(x-x_0)}{d(x)}}\right);$$

$$s_1 = 0; \left(e^{\frac{(x-x_0)}{d(x)}}\right)\left(1 + e^{\frac{(x-x_0)}{d(x)}}\right) = 0; \; e^{\frac{(x-x_0)}{d(x)}} = -1$$

So S1 cannot be zero.

$$s_{2=}\left(-\left(1 + e^{\frac{(x-x_0)}{d(x)}}\right)\right) + 2e^{\frac{(x-x_0)}{d(x)}};$$

$$s_{2=}0; 2e^{\frac{(x-x_0)}{d(x)}} - \left(1 + e^{\frac{(x-x_0)}{d(x)}}\right) = 0;$$

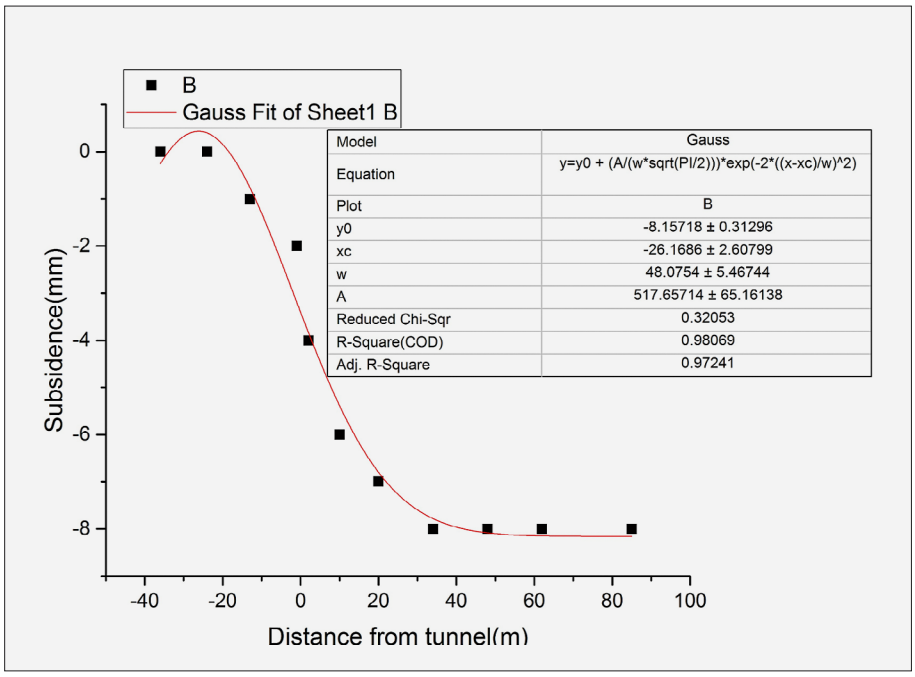

Figure 3. Subsidence profile represented using a Gaussian function

$$2e^{\frac{(x-x_0)}{d(x)}}=\left(1+e^{\frac{(x-x_0)}{d(x)}}\right);(2-1)e^{\frac{(x-x_0)}{d(x)}}=1;$$

$$if\ (2-1)=m;\ e^{\frac{(x-x_0)}{d(x)}}=\frac{1}{m};$$

$$\frac{(x-x_0)}{d(x)}=Ln\frac{1}{m};\ x=dx\left(\ln\frac{1}{m}\right)+x_0;$$

$$Ln\ 1=0;\ x=dx\left(\ln\frac{1}{(2-1)}\right)+x_0;\ x=x_0;\ i=x_0 \quad (1)$$

Using the Boltzmann function analysis, the inflection point, denoted as i = x0, was identified. Additionally, the total of the maximum subsidence and the subsidence values was outlined as **Equations 2** and **3**.

$$s_{max}=A_1-A_2 \quad (2)$$

$$s=A_2+\frac{s_{max}}{2} \quad (3)$$

where A1 represents the initial volume or area, and A2 denotes the reduced volume or area.

$$y=y_0+\left(\frac{A}{w*\sqrt{\frac{\pi}{2}}}\right)*e^{\left[-2\left(\frac{x-x_C}{w}\right)^2\right]}:\ y=k*e^{f(x)}:$$

$$y=y_0+k*e^{f(x)}:\ k=\frac{A}{w*\sqrt{\frac{\pi}{2}}}:$$

$$F_{(x)}=-2\left(\frac{x-x_C}{w}\right)^2=-2\left[\frac{1}{\omega}x-\frac{x_c}{w}\right]^2:$$

$$y'=K*f'_{(x)}*e^{f(x)}:\ f'_{(x)}=\frac{-4}{w}\left[\frac{x-x_c}{w}\right]:$$

$$y'=\frac{-4k}{w}\left[\frac{x-x_c}{w}\right]e^{\left[-2\left(\frac{x-x_C}{w}\right)^2\right]}:\ g_{(x)}=\frac{-4k}{w}\left[\frac{x-x_c}{w}\right]:$$

$$h_{(x)}=e^{\left[-2\left(\frac{x-x_C}{w}\right)^2\right]}:$$

$$y'=g_{(x)}\cdot h_{(x)}:\ y''=g'h+h'g:\ g'=\frac{-4k}{w}\left[\frac{1}{w}\right]$$

$$h'=\frac{-4}{w}\left[\frac{x-x_c}{w}\right]e^{\left[-2\left(\frac{x-x_C}{w}\right)^2\right]}$$

$$y''=\frac{-4k}{w^2}e^{-2\left(\frac{x-x_C}{w}\right)^2}+\frac{16k}{w^4}(x-x_c)^2e^{-2\left(\frac{x-x_C}{w}\right)^2}$$

$$y''=\left[\frac{4k}{w^2}e^{-2\left(\frac{x-x_C}{w}\right)^2}\right]\left[\frac{4}{w^2}(x-x_c)^2-1\right]=0$$

$$s_1=\frac{4k}{w^2}e^{-2\left(\frac{x-x_c}{w}\right)^2}$$

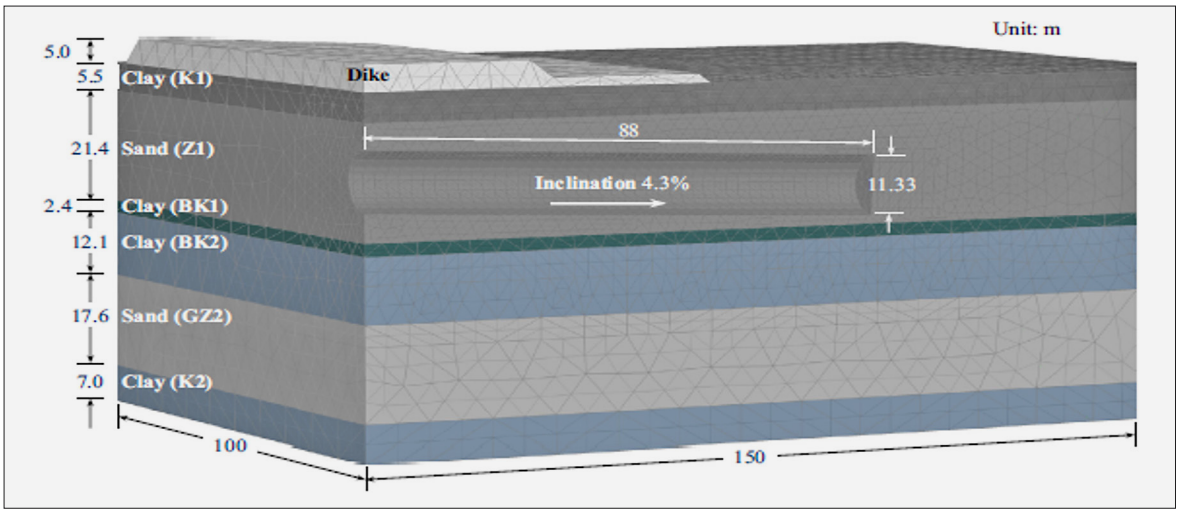

Figure 4. Tunnel geometry and soil stratification for validating numerical models with data collected from the Western Scheldt tunnel project

Table 4. Geomechanical properties of soil layers at the Western Scheldt tunnel project site

Parameter	Soil Layers						
	Dike	K1	Z1	BK1	BK2	GZ2	K2
γ_{unsat} (kN/m³)	19	18	18	18	17	17	17
γ_{sat} (kN/m³)	20	20	19	21	19.3	20.2	20
φ' (deg.)	28	22	30	28	28	34	35
ψ (deg.)	0	0	0	0	0	4	0
c' (kPa)	5	5	6.4	20	20	11.4	40
K_0^{nc} (-)	0.53	0.63	0.50	0.53	0.53	0.40	0.36
E_{50}^{ref} (kPa)	30000	24000	35000	25000	30000	30000	50000
E_{oed}^{ref} (kPa)	30000	24000	35000	25000	30000	30000	50000
E_{ur}^{ref} (kPa)	90000	60000	80000	60000	100000	90000	180000
ν_{ur} (-)	0.20	0.20	0.20	0.20	0.20	0.20	0.20
OCR (-)	1.0	1.0	1.0	2.7	2.8	2.5	3.0
G_0^{ref} (kPa)	160000	150000	140000	65000	100000	110000	150000
$\gamma_{0.7}$ (-)	0.0002	0.0002	0.0002	0.0002	0.0002	0.0002	0.00015
p^{ref} (kPa)	100	100	100	100	100	100	100
m (-)	0.7	0.7	0.5	0.7	0.7	0.5	0.7
R_f (-)	0.90	0.9	0.9	0.9	0.9	0.9	0.9

$$s_2 = \frac{4}{w^2}\left(x - x_c\right)^2 - 1$$

$$If s_2 = 0 \Rightarrow \frac{4}{w^2}\left(x - x_c\right)^2 = 1:$$

$$\left(x - x_c\right)^2 = \frac{W^2}{4} \Rightarrow \left(x - x_c\right) = \pm\frac{W}{2}$$

$$x = \pm\frac{W}{2} + x_c \qquad (4)$$

The diagram of the Gaussian function, derived from the data in **Table 3**, is illustrated in **Figure 3**. An inflection point was generated through the dual effect of the derivative of the given formula. From the analysis of the Gaussian function, the inflection point $i = \pm\frac{W}{2} + x_c$ was identified, and the total of the maximum subsidence and subsidence was defined as **Equations 5** and **6**.

$$S_{max} = \frac{A}{w * \sqrt{\frac{\pi}{2}}} \qquad (5)$$

$$s = s_{max} * e^{-0.5} \qquad (6)$$

where A represents the initial excavated volume (or area), and $w * \sqrt{\frac{\pi}{2}}$ denotes the final excavated volume (or area).

2.5. *Numerical Modelling*

2.5.1. Validation of Numerical Modelling

Numerical modelling for the twin tunnels project beneath the Scheldt River in the Netherlands was validated using the finite element method through Plaxis 3D software. **Figure 4** illustrates the tunnel geometry and soil stratification, while **Table 4** provides the geomechanical properties of the soil.

Table 5 presents the material specifications utilized to represent the final concrete cover and the TBM cover, while Figure 5 displays the tunnel with the TBM positioned at its ultimate location. In the illustration, the final concrete cover of the tunnel is shown via white elements, and the cover components of the machine are highlighted using bold blue panels. The applied slurry pressure on the soil at both the excavation face and the tail end of the machine prior to the completion of the final concrete cover is also distinctly visible.

Table 5. Specifications of the final concrete tunnel lining and TBM machine lining in numerical modelling

Parameter	Tunnel lining	TBM shield
γ (kN/m^3)	24	38
E (kPa)	2.2E7	2.1E8
Thickness D (m)	0.45	0.35
ν (-)	0.2	0.3

After performing the finite element analysis, the ground settlement changes obtained from the analysis were compared with the results of the modelling measurements conducted by **Zhao et al. (2015)**. **Figure 6** illustrates the ground settlement in the longitudinal and transverse directions. As shown in this figure, there is relatively good agreement between the modelling results in the present study and the measured settlement values, as well as the settlement values obtained from numerical modelling by previous researchers.

3. Results and Discussion

3.1. *Numerical Modelling*

Given that the accuracy of the numerical modelling using the above model is positively evaluated, the next step involves creating the numerical models required for the studies in question using the assumptions and modelling method outlined above. The modelling was conducted using the hardening soil model (HS-S) with small strain for the excavation site of the twin tunnels of the Isfahan Metro at the Si-o-se-pol section, along with three other soil models. The parameters employed in this modelling are shown in **Tables 6**, **7** and **8**.

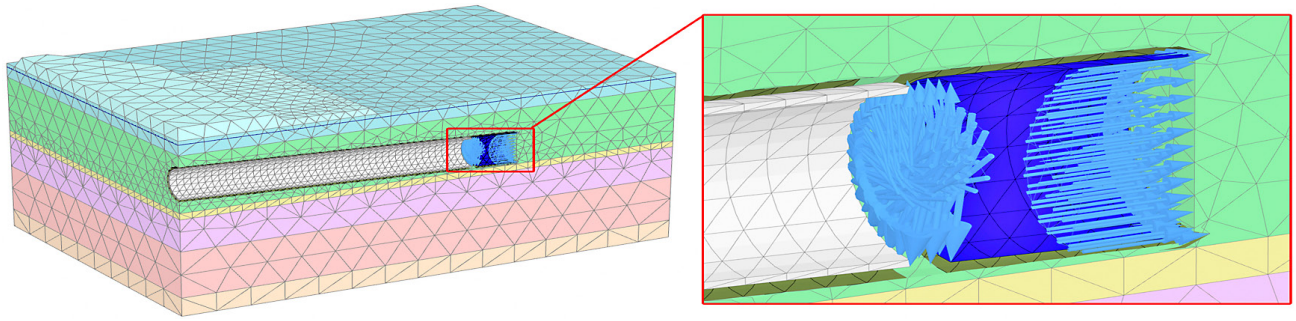

Figure 5. Geometry of the numerical finite element model of the Western Scheldt tunnel project

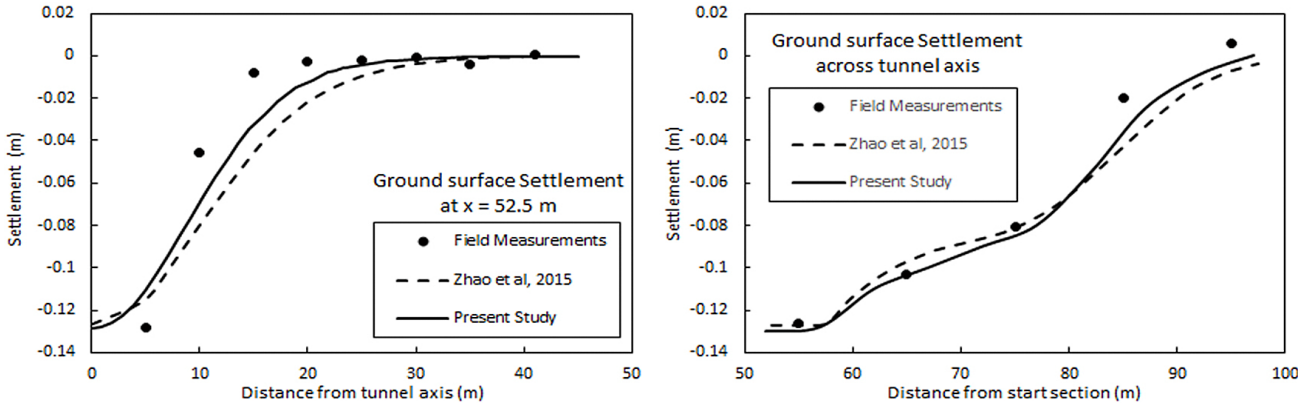

Figure 6. Comparison of the results obtained from the land surface settlement in the longitudinal (right figure) and transverse (left figure) directions in the numerical model and comparison or measurements made in the Western Scheldt tunnel project and the numerical model of **Zhao et al. (2015)**

Table 6. Behavioural parameters studied in sensitivity analyses on the Si-o-se-pol section

E_{50}^{ref} (MPa)	φ (deg.)	c (kPa)	γ_{sat} (kN/m^3)	Tunnels spacing ratio s/D (m)	Tunnels depth ratio H/D (m)
15	10	2	16	1.25	1.2
40	30	10	17.5	2.6	2
65	36	20	19	4	3

Table 7. Geometric parameters studied in different numerical modelling

Soil Types	Tunnels spacing ratio s/D (m)	Tunnels depth ratio H/D (m)
Soil 1	1.25	1
Soil 2	1.5	2
Soil 3	2	3

and the extensive dimensions of the numerical model, using finer meshing significantly increases the calculation time to an extent that it poses considerable challenges in conducting the studies.

Figure 9 illustrates the tunnel progress from the beginning to the completion of excavation. As shown in this figure, the right-hand tunnel is excavated first, followed by the excavation of the left-hand tunnel once the right-hand tunnel is completed. The tunnel progress modelling process was consistent across all models and was similar to the one used for validation. Since it is not feasible to model only part of the geometry in the case of twin tunnels, the entire tunnel cross-section geometry must be modelled. To depict the portion of the tunnel being excavated, sections need to be created to visualize the internal activity within the model. For this purpose, horizontal and vertical sections have been created in the figure below to better illustrate the tunnel excavation process.

Table 8. Geomechanical parameters of materials used in the analyses

Parameter	Soil 1	Soil 2	Soil 3	Tunnel lining	TBM shield
γ (kN/m^3)	19	18	17	24	38
E_{50}^{ref} (kPa)	70000	35000	15000	2.2E7	2.1E8
m	0.3	0.5	0.7		
φ' (deg.)	36	30	24	-	-
ψ (deg.)	6	0	0	-	-
c' (kPa)	2	10	20	-	-
G_0^{ref} (kPa)	180000	90000	40000	-	-
$\gamma_{0.7}$	0.0002	0.0002	0.0002	-	-
ν (-)	-	-	-	0.2	0.3
Thickness D (m)	-	-	-	0.25	0.35

3.1.1. Geometry and meshing of models

Figure 7 shows the geometric dimensions of the model parametrically. As seen in this figure, the distance from the axis of each tunnel to the lateral boundaries of the model is considered to be 5 times the diameter of the tunnel. Additionally, the depth of the bedrock, or the depth at which the deformations caused by tunnel excavation become negligible, is located at a distance of 3 times the diameter below the bottom of the tunnel. Considering that the parameter for the ratio of the distance between the tunnels is s/D and the parameter for the ratio of the depth of the tunnels is H/D, the dimension of the model in the horizontal direction perpendicular to the tunnel axis is equal to (10+s/D)*D, and in the vertical direction is equal to (4+H/D)*D.

The meshing of the model has been performed in a manner that ensures the speed of the model analysis is acceptable, while maintaining that the solutions are not influenced by the size of the elements. For this purpose, finer elements have been applied around the tunnels and coarser elements at more distant points. **Figure 8** illustrates the meshing of a sample of the models. It is worth mentioning that, due to the modelling of the tunnel's progression stages, the large number of analysis stages,

The numbering of the excavation stages is structured so that the initial stresses in the soil are first modelled before the tunnel excavation begins. Subsequently, the first tunnel is excavated in 27 stages, with each stage progressing in 2-meter increments. The initial location of the tunnel is chosen such that, given the 2-meter distance between the end of the TBM and the last installed lining segment, the head of the machine is positioned 18 meters from the beginning of the model. The section under study for settlement investigation is located 30 meters from the start of the model. A total of 26 excavation stages corresponds to 52 meters of tunnel advancement, completing the excavation process for each line. Therefore, at the conclusion of the excavation, the head of the TBM will be situated 70 meters from the beginning of

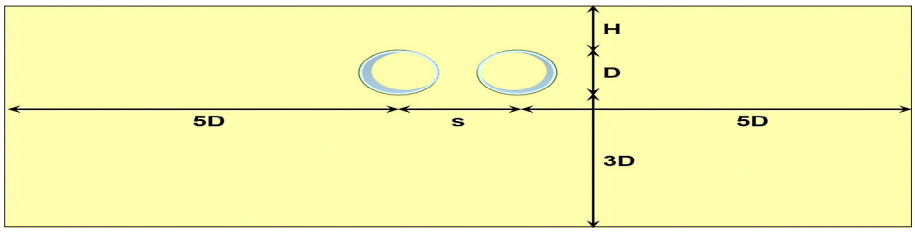

Figure 7. Parametric geometry of numerical models

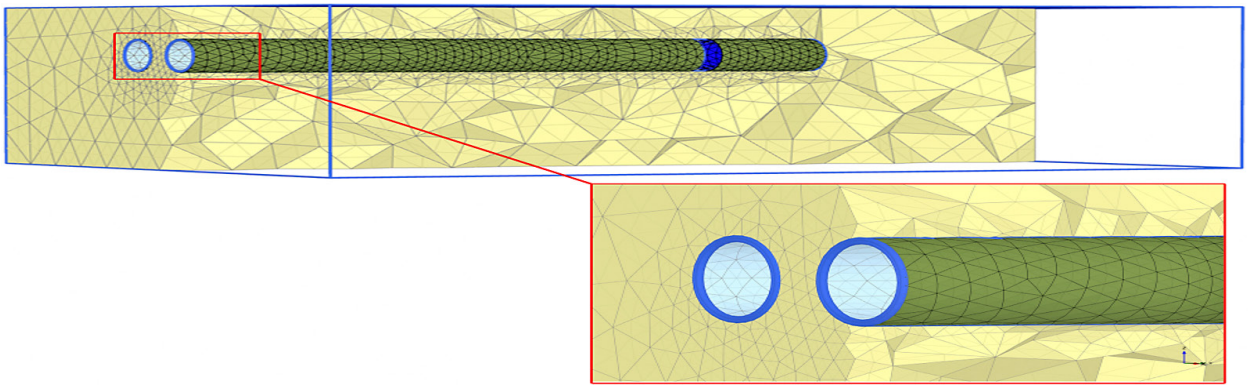

Figure 8. Elementing of numerical models

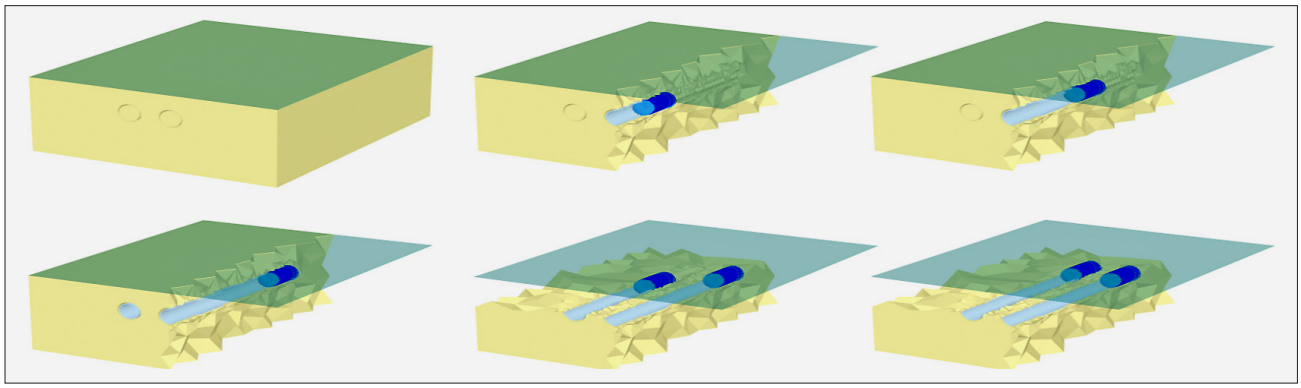

Figure 9. Modelling the progress of twin tunnels in different stages including: stage zero (top left row), stage two at the beginning of the first tunnel excavation (top middle row), stage 12 in the middle of the first tunnel excavation (top right row), stage 27 after the completion of the first tunnel excavation and at the beginning of the second tunnel excavation (bottom left row), stage 37 in the middle of the second tunnel excavation (bottom middle row) and stage 54 at the end of the second tunnel excavation (bottom right row)

the model. To mitigate boundary effects, the model's longitudinal dimension in the direction of the tunnels is set to 100 meters. A similar process as described above is followed for the excavation of the second tunnel. Consequently, the total number of analysis stages amounts to 54. As illustrated in the figure above, prior to the excavation of the second tunnel, the soil elements within this tunnel remain active. As the excavation progresses, the soil elements along the tunnel's longitudinal direction are deactivated. The pressure values used for each model, based on the tunnel's depth, are selected to prevent significant deformations during excavation. In models where the tunnel depth is 1.0D, the slurry pressure at the excavation face starts at 90 kPa at the upper part and increases linearly at a rate of 15 kPa/m. For models where the tunnel depth is 2 and 3 times the tunnel diameter, the pressure at the upper part of the cross-section is set to 180 and 270 kPa, respectively, while the pressure increase with depth remains consistent at 15 kPa/m across all models. In the case of slurry.

3.1.2. Numerical Modelling (Comparison of numerical modelling with M-C and HS-S models)

Using three-dimensional Plaxis software and considering the Hardening Soil model with small strain (HS-S) and Mohr-Coulomb (M-C) behavioural models, the total subsidence was analyzed for the excavation of the twin metro tunnel at Si-o-se-pol station in Isfahan. As shown in **Figures 10** to **12,** the use of the M-C behavioural model results in unreasonable heave at the ground surface. This

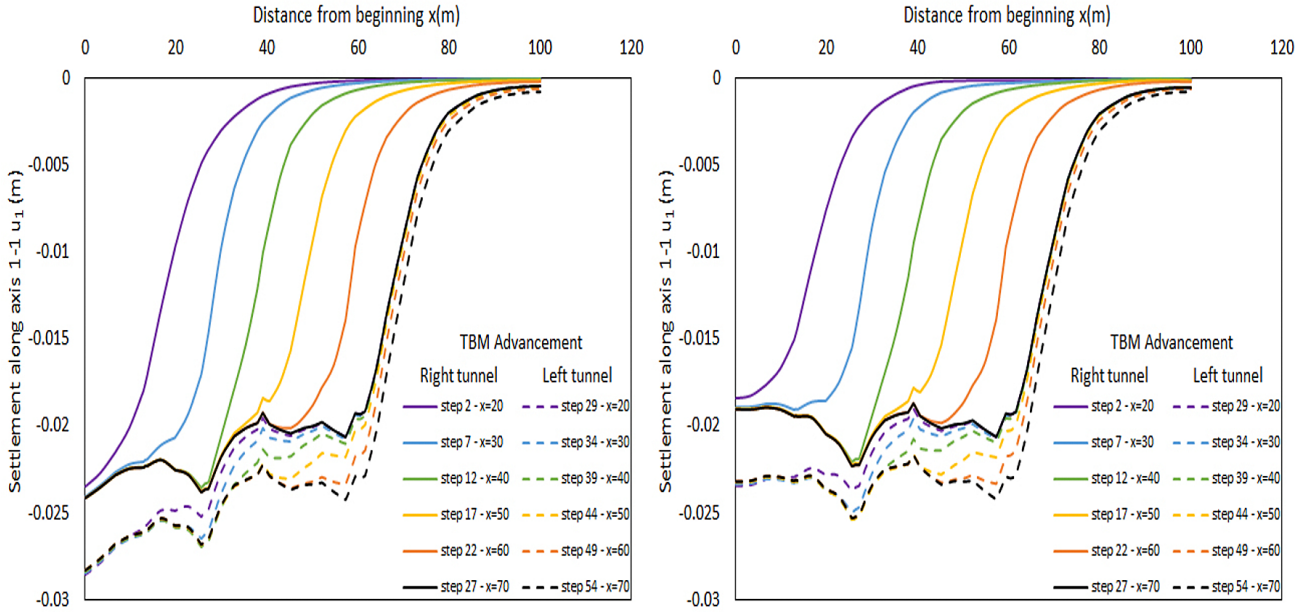

Figure 10. Results of ground settlement with M-C and HS-S models along the longitudinal axis of Si-o-se-pol first tunnel.

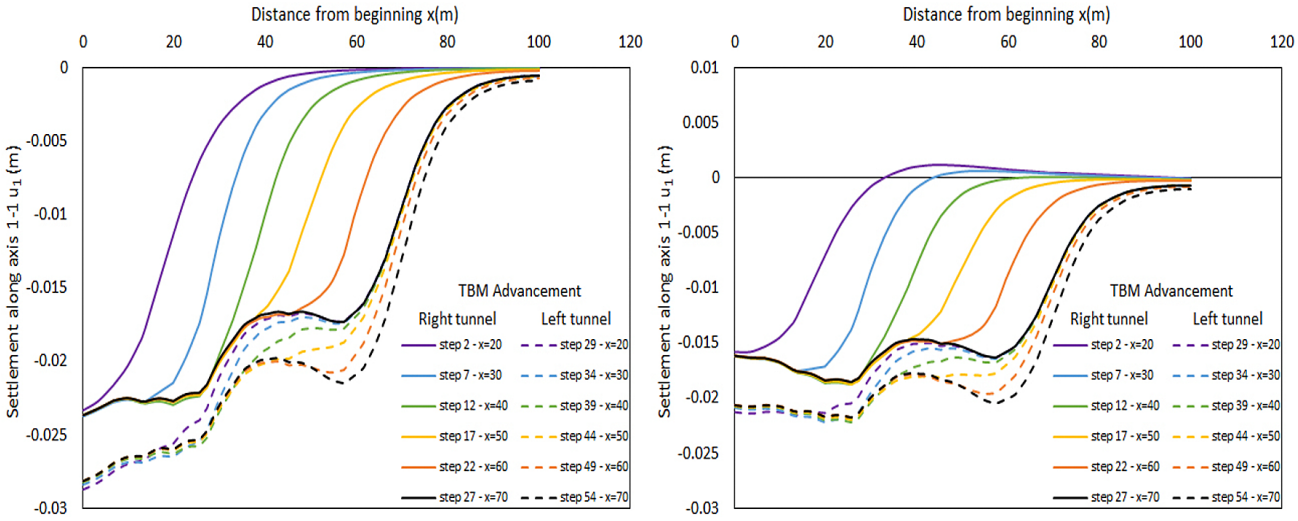

Figure 11. Results of ground settlement with M-C and HS-S models at the end of Si-o-se-pol first tunnel.

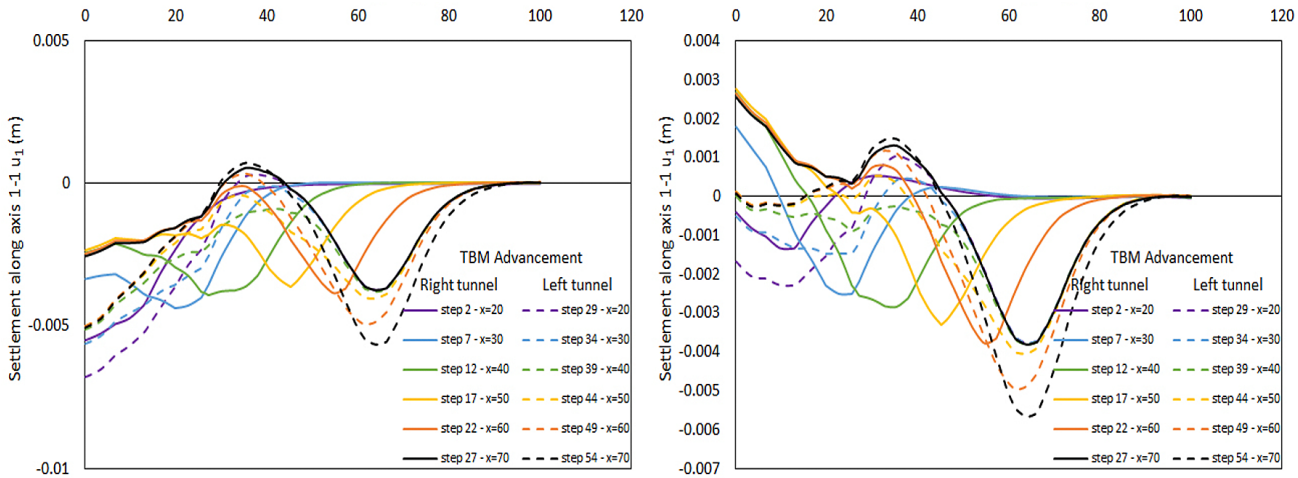

Figure 12. Results of ground settlement with M-C and HS-S models at the end of Si-o-se-pol second tunnel.

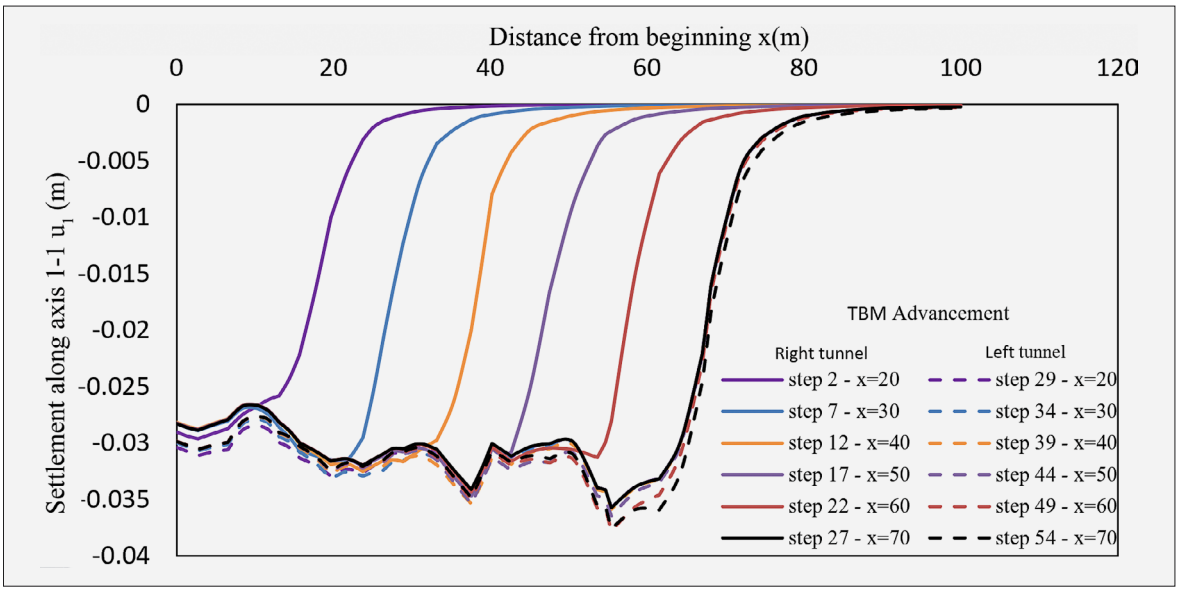

Figure 13. Numerical Analysis of subsidence with Plaxis 3D for Si-o-se-pol station

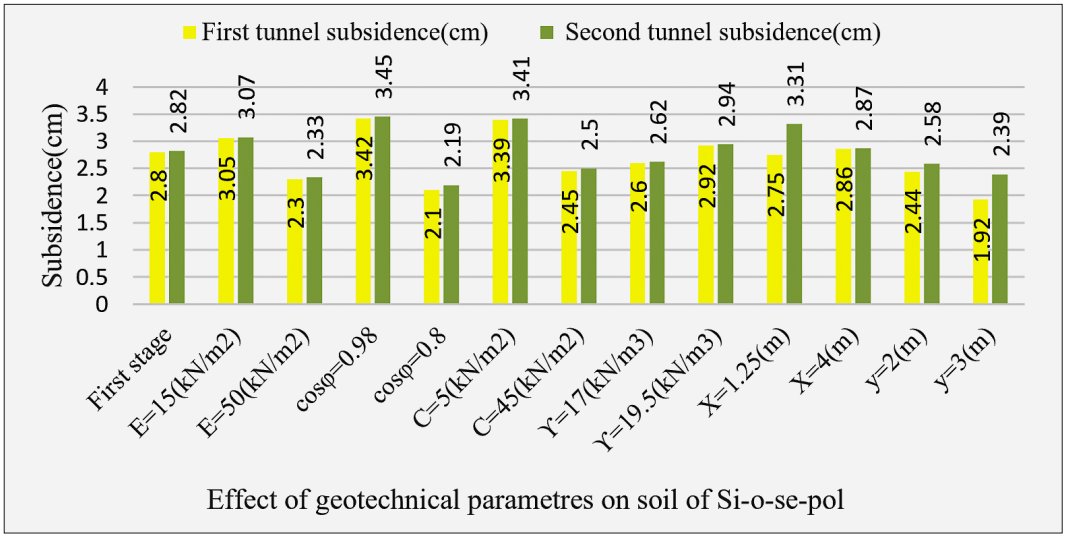

Figure 14. Results of numerical analysis with Plaxis 3D for Si-o-se-pol station

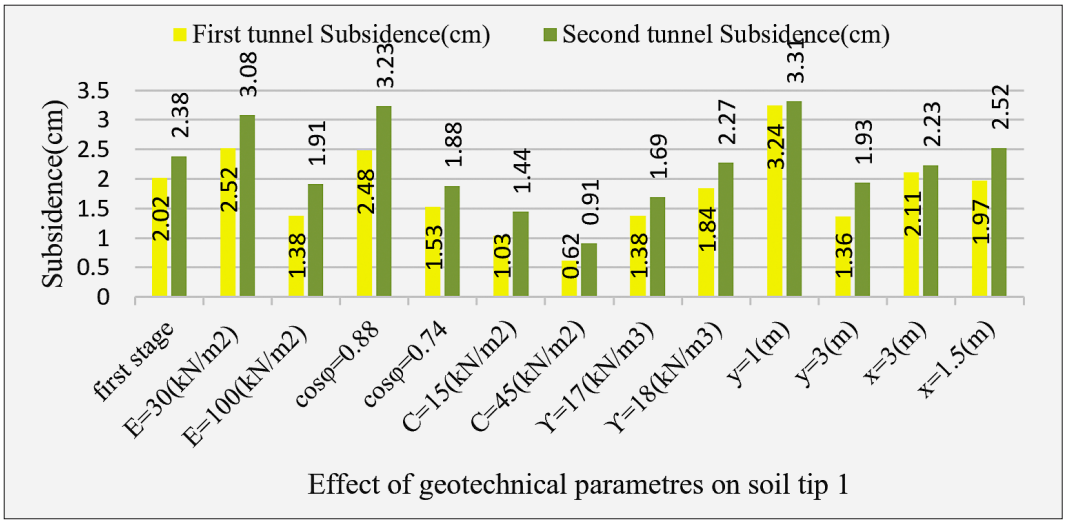

Figure 15. Results of numerical analysis with Plaxis 3D for soil tip 1

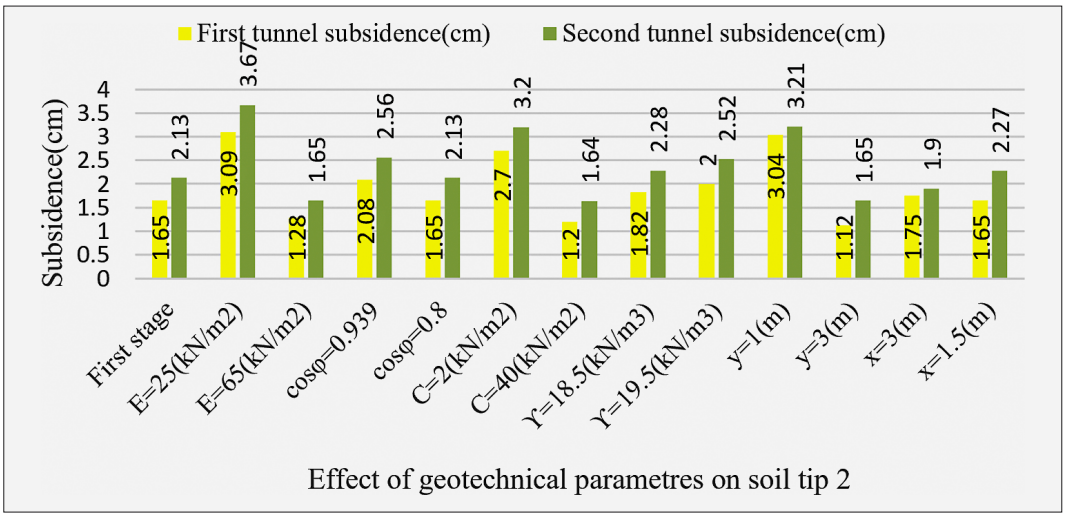

Figure 16. Results of numerical analysis with Plaxis 3D for soil tip 2

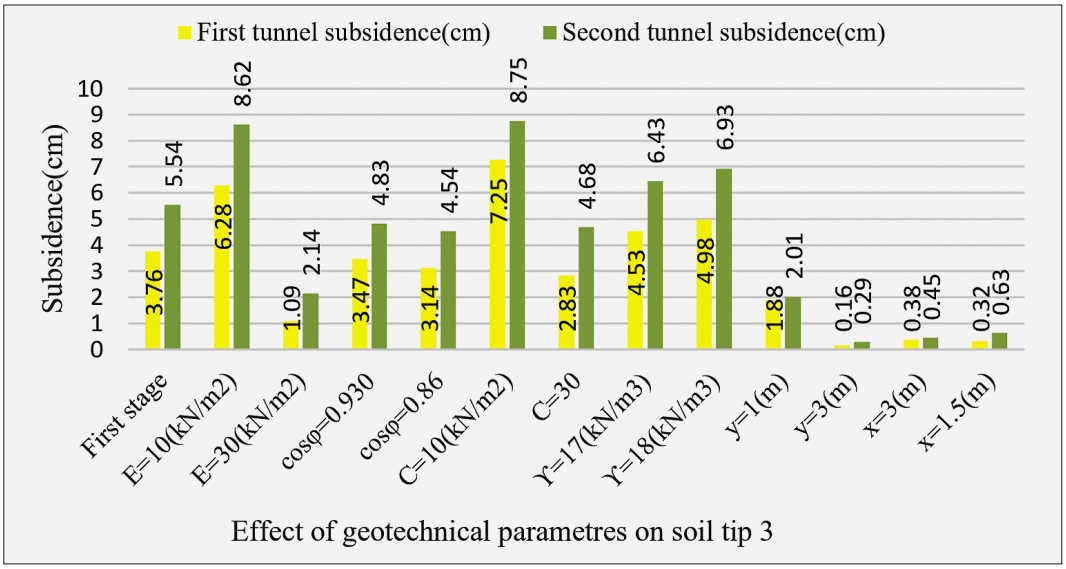

Figure 17. Results of numerical analysis with Plaxis 3D for soil tip 3

is primarily because, in the M-C model, the loading and unloading moduli are considered identical, whereas in the HS-S behavioural model, these moduli are defined separately and depend on the overall stress level. To compare the results obtained from the HS-S behavioural model and the Mohr-Coulomb (M-C) model, the settlement results along the longitudinal axis of Si-o-se-pol's first tunnel, at the end of the excavation of Si-o-se-pol's first tunnel, and at the end of the excavation of Si-o-se-pol's second tunnel were analyzed and compared.

3.1.3 Numerical Modelling Results by Hardening soil model with Small Strain (HS-S)

As shown in **Figure 13**, the maximum subsidence rate determined after the second tunnel was excavated.

In order to provide a numerical relationship, the effective parameters on the soil subsidence of the twin tunnel excavation for the Si-o-se-pol station and three other soil types were analyzed using three-dimensional Plaxis software (see **Figure 14** to **Figure 19**).

3.1.4 Numerical Modelling based on Genetic algorithms (GA)

The results of the numerical analysis were sensitivity-analyzed for four types of soil using the genetic algorithm (see **Figure 20**), and a numerical relationship was established.

In the end, numerical **Equation 7** was proposed for the maximum subsidence by the genetic algorithm. The sum of the A and B parameters is shown in **Table 9**.

$$s_{\max} = A\left(\frac{(y*\gamma)-(C*x)}{E}*\cos\varphi\right)^{B} \quad (7)$$

The empirical formula, based on the Boltzmann function, indicates the subsidence, the maximum subsidence, and the inflection point of the following **Equation 8**.

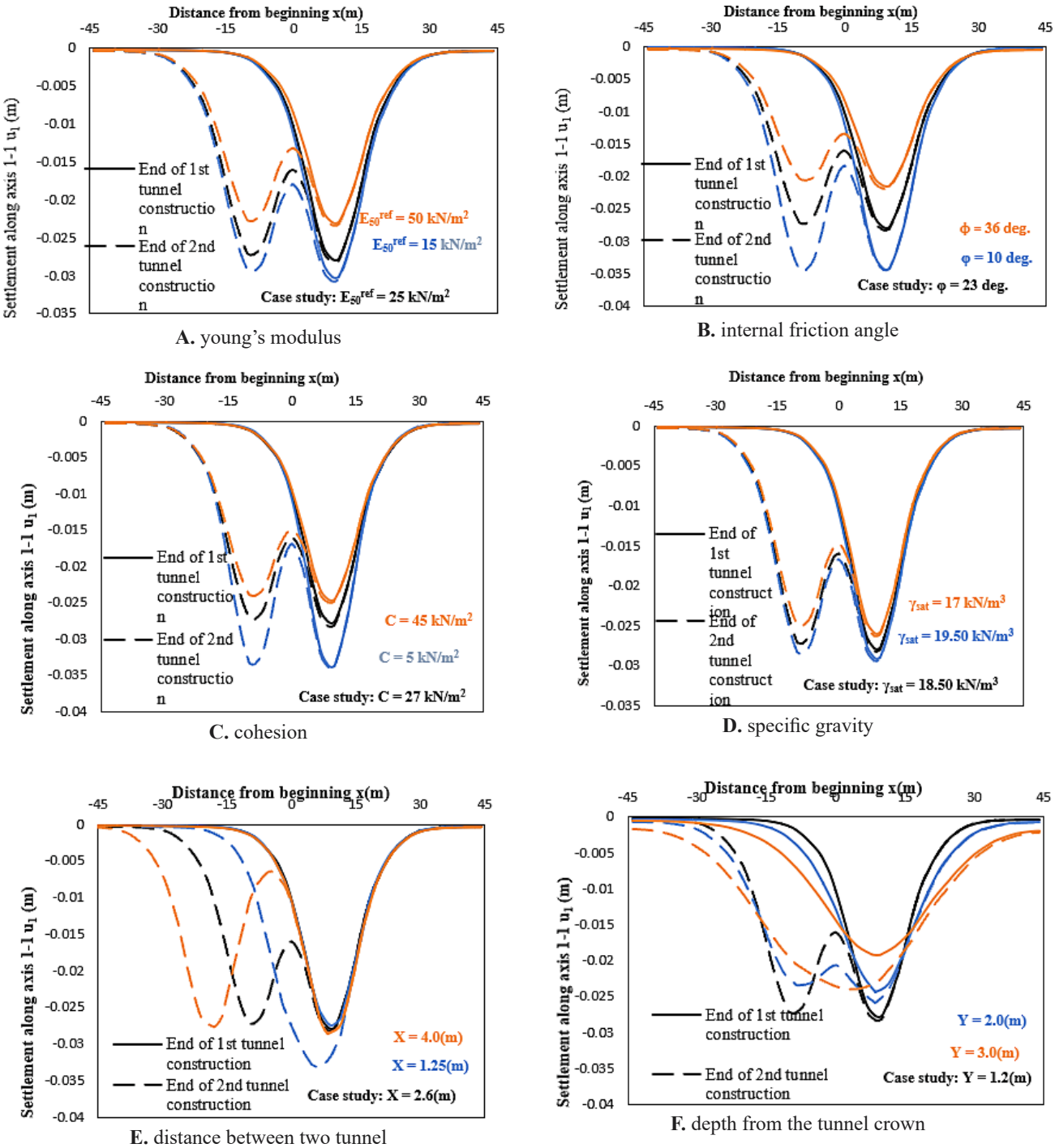

A. young's modulus

B. internal friction angle

C. cohesion

D. specific gravity

E. distance between two tunnel

F. depth from the tunnel crown

Figure 18. Sensitivity analysis of effective parameters of soil subsidence in Si-o-se-pol station.

$$s = A_2 + \frac{S_{max}}{2};\ s_{max} = A_1 - A_2;\ i = x_0 \qquad (8)$$

Prediction of the settlement of twin tunnels using experimental and numerical formulas is illustrated in **Figure 21**.

4. Conclusions

This study examines the earth's surface subsidence caused by tunnel excavation, utilizing the results of the survey. Based on the results obtained from the empirical formulation, we provide the maximum subsidence and inflection point curve. The recording of results using the NAK2 camera has been conducted to enhance the accuracy of the results per unit time, with two photo indices and corresponding information recorded. Additionally, by increasing the frequency of monitoring and data recording, highly favourable results have been achieved. A strong correlation is observed between the maximum subsidence recorded during the earth's monitoring and

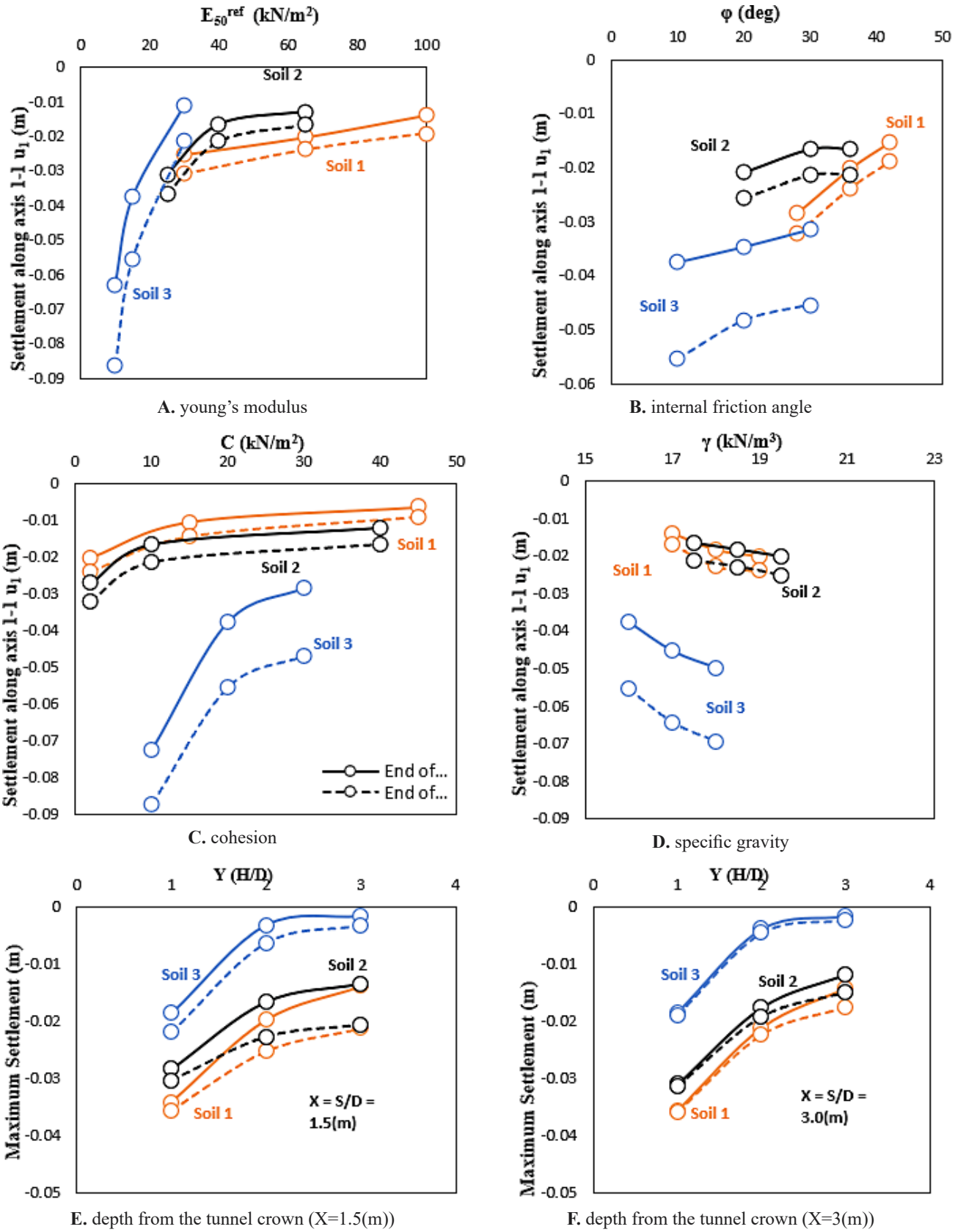

Figure 19. Sensitivity analysis of effective parameters of soil subsidence in 3 types of soil.

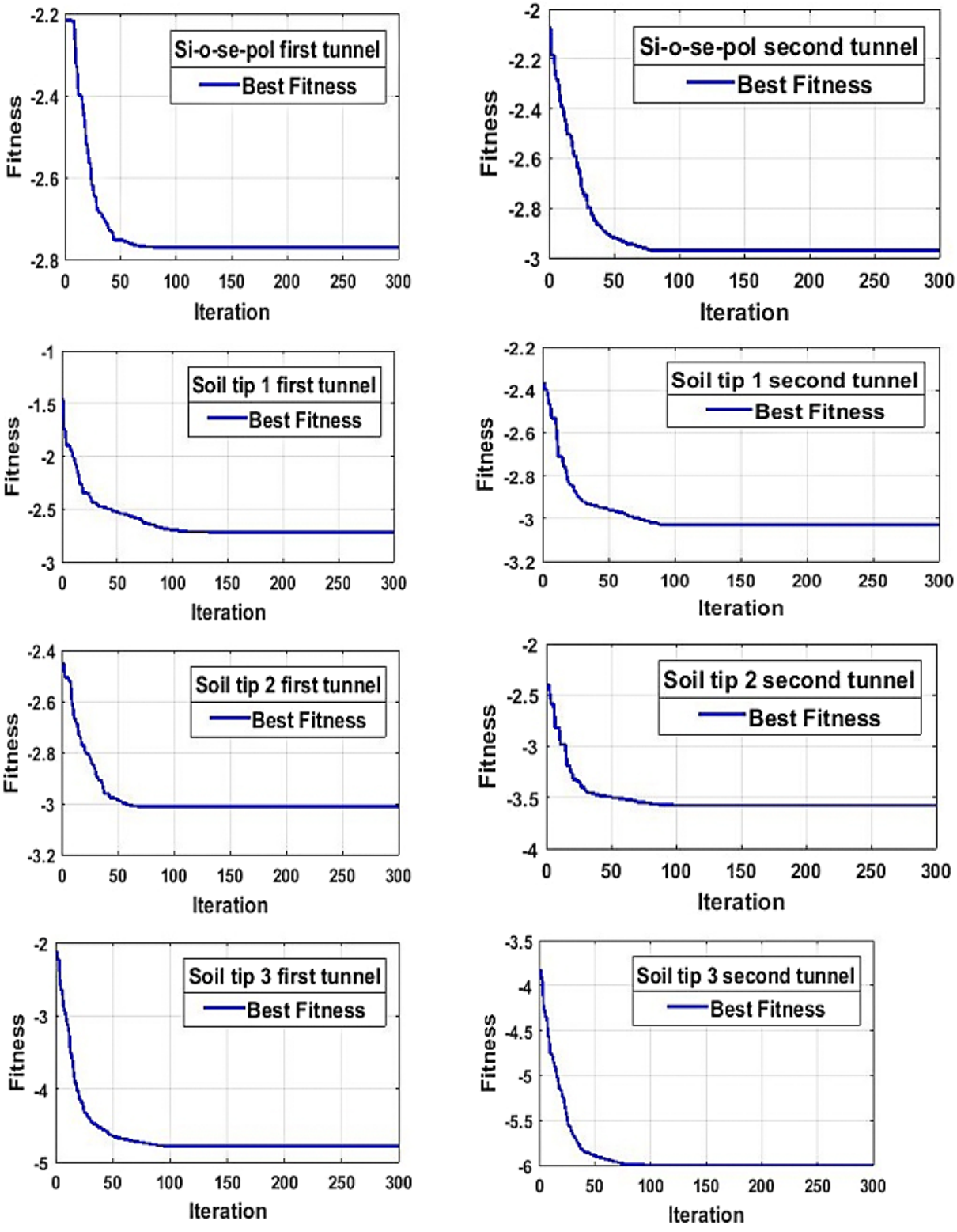

Figure 20. The sum of the subsidence obtained by the genetic algorithm

the maximum subsidence and inflection point obtained from both experimental formulas.

Furthermore, the comparison of two behavioural models indicates that numerical analysis with the M-C behavioural model results in unreasonable uplift at the ground surface. This is primarily because, in the M-C model, the loading and unloading moduli are assumed to be identical, whereas, in the HS-S behavioural model, the loading and unloading moduli are defined separately and are dependent on the all-around stress level.

In this research, using three-dimensional Plaxis software and the HS-S model, the parameters influencing

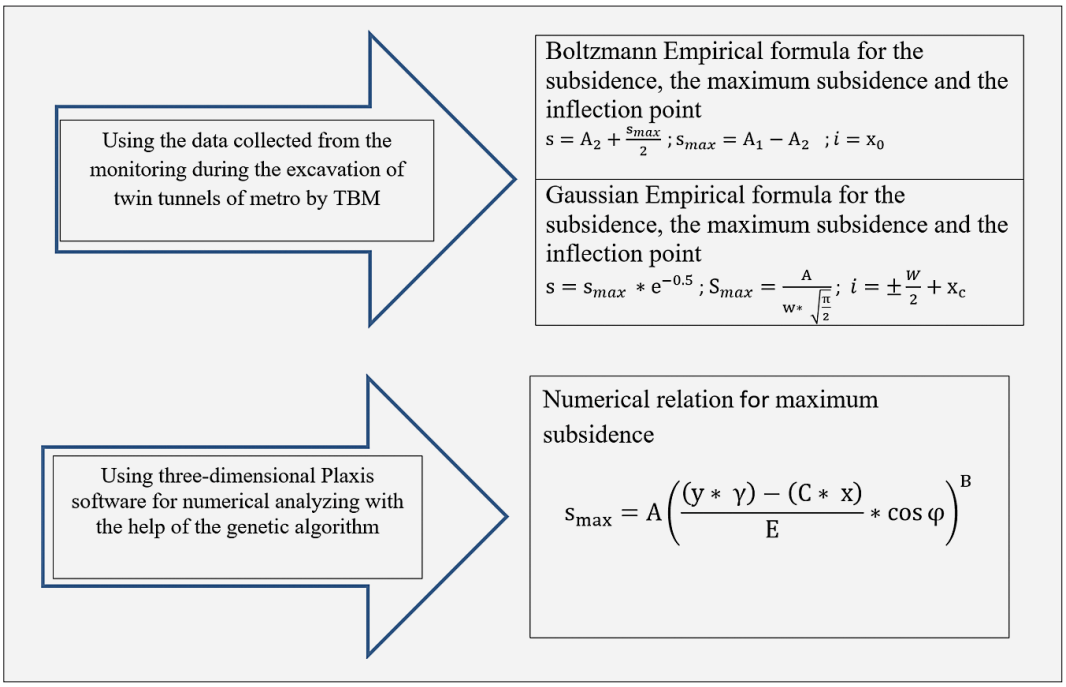

Figure 21. Prediction of settlement of twin tunnels using experimental and numerical formula

Table 9. The sum of the maximum subsidence obtained by the numerical formula obtained by the genetic algorithm

Si-o-se-pol	A=676 B=0.493	s_{max} = 2.9719
Soil tip 1 (Soil Identification & Classification: GW)	A=997 B=0.416	s_{max} = 3.0294
Soil tip 2 (Soil Identification & Classification: CL-SM)	A= 893 B= 0.293	s_{max} = 3.5762
Soil tip 3 (Soil Identification & Classification: CL)	A= 472 B= 0.714	s_{max} = 5.9984

soil subsidence were analyzed for sensitivity concerning the Si-o-se-pol and three types of soil, employing a genetic algorithm. Consequently, due to the close correlation between the empirical and numerical relationships derived in this study, it is feasible to estimate the ground subsidence for Isfahan Metro Line 2, which is currently under excavation.

5. References

Ahmed, K. S., Sharmin, J., & Ansary, M. A. (2023). Numerical investigation of tunneling induced surface movement: A case study of MRT line 1, Dhaka. Underground Space, 12, 116-136. https://doi.org/10.1016/j.undsp.2023.02.008

Alsirawan, R., Sheble, A., & Alnmr, A. (2023). Two-dimensional numerical analysis for TBM tunneling-induced structure settlement: A proposed modeling method and parametric study. Infrastructures, 8(5), 88. https://doi.org/10.3390/infrastructures8050088

Andrab, S. G., Hekmat, A., & Yusop, Z. B. (2017). A review: evolutionary computations (GA and PSO) in geotechnical engineering. *Computational Water, Energy, and Environmental Engineering*, *6*(2), 154-179. DOI: 10.4236/cweee.2017.62012

Arioglu E (1992) Surface movements due to tunneling activities in urban areas and minimization of building damages. Short Course, Istanbul Technical University, Mining Engineering Department (in Turkish). DOI:10.1007/s12665-010-0530-6.

Attewell, P. B., Yeates, J., Selby, A.R., 1986. Soil Movements Induced by Tunnelling. Chapman & Hall, New York.

Basarir, H., Genis, M., & Ozarslan, A. (2010). The analysis of radial displacements occurring near the face of a circular opening in weak rock mass. International Journal of Rock Mechanics and Mining Sciences, 47 (2010), 771-783. https://doi.org/10.1016/j.ijrmms.2010.03.010

Benayoun, F., Boumezerane, D., Bekkouche, S. R., & Bendada, L. (2020, March). Application of genetic algorithm method for soil nailing parameters optimization. In IOP Conference Series: Materials Science and Engineering (Vol. 800, No. 1, p. 012009). IOP Publishing. DOI: 10.1088/1757-899X/800/1/012009

Chakeri, H., Ozcelik, Y., & Unver, B. (2013). Effects of important factors on surface settlement prediction for metro tunnel excavated by EPB. Tunnelling and Underground Space Technology, 36, 14-23. Chakeri, H., Ozcelik, Y., & Unver, B. (2013). Effects of important factors on surface settlement prediction for metro tunnel excavated by EPB. Tunnelling and Underground Space Technology, 36, 14-23. https://doi.org/10.1016/j.tust.2013.02.002

Chakeri, H., & Ünver, B. (2014). A new equation for estimating the maximum surface settlement above tunnels excavated in soft ground. Environmental earth sciences, 71, 3195-3210. https://doi.org/10.1007/s12665-013-2707-2

Chapman, D. N., Ahn, S. K., & Hunt, D. V. (2007). Investigating ground movements caused by the construction of mul-

tiple tunnels in soft ground using laboratory model tests. Canadian Geotechnical Journal, 44(6), 631-643. https://doi.org/10.1139/t07-018

Chen, S. L., Lee, S. C., & Wei, Y. S. (2016). Numerical analysis of ground surface settlement induced by double-o tube shield tunneling. Journal of Performance of Constructed Facilities, 30(5), 04016012. DOI: 10.1061/(ASCE)CF.1943-5509.0000732

Cui, L., & Sheng, D. (2005). Genetic algorithms in probabilistic finite element analysis of geotechnical problems. Computers and Geotechnics, 32(8), 555-563. https://doi.org/10.1016/j.compgeo.2005.11.005

Das, R., Singh, P. K., Kainthola, A., Panthee, S., & Singh, T. N. (2017). Numerical analysis of surface subsidence in asymmetric parallel highway tunnels. Journal of Rock Mechanics and Geotechnical Engineering, 9(1), 170-179. https://doi.org/10.1016/j.jrmge.2016.11.009

Fang, Y., He, C., Nazem, A., Yao, Z., & Grasmick, J. (2017). Surface settlement prediction for EPB shield tunneling in sandy ground. KSCE Journal of Civil Engineering, 21, 2908-2918. https://doi.org/10.1007/s12205-017-0989-8

Fang, Y., Yang, Z., Cui, G., & He, C. (2015). Prediction of surface settlement process based on model shield tunnel driving test. Arabian Journal of Geosciences, 8, 7787-7796. DOI:10.1007/s12517-015-1800-0

González, C., & Sagaseta, C. (2001). Patterns of soil deformations around tunnels. Application to the extension of Madrid Metro. Computers and Geotechnics, 28(6-7), 445-468. https://doi.org/10.1016/S0266-352X(01)00007-6

He, C., Feng, K., Fang, Y., & Jiang, Y. C. (2012). Surface settlement caused by twin-parallel shield tunnelling in sandy cobble strata. Journal of Zhejiang University SCIENCE A, 13(11), 858-869. DOI:10.1631/jzus.A12ISGT6

Herzog M (1985) Surface subsidence above shallow tunnels (in German). Bautechnik 62:375–377

Hasanpour, R. (2014). Advance numerical simulation of tunneling by using a double shield TBM. Computers and Geotechnics, 57, 37-52. https://doi.org/10.1016/j.compgeo.2014.01.002

Jaberi, A., & Zare, S. (2023). Investigating the effect of different soil parameters in different behavior models on prediction of settlement induced by tunneling (Case study: Qom metro lineA). Journal of Mining Engineering, 18(58), 15-35. https://doi.org/10.22034/ijme.2022.549390.1906

Jin, Y. F., Yin, Z. Y., Shen, S. L., & Zhang, D. M. (2017). A new hybrid real-coded genetic algorithm and its application to parameters identification of soils. Inverse Problems in Science and Engineering, 25(9), 1343-1366. https://doi.org/10.1080/17415977.2016.1259315

Khoshzaher, E., Chakeri, H., Bazargan, S., & Mousapour, H. (2023). The prediction of EPB-TBM performance using firefly algorithms and particle swarm optimization. Rudarsko-geološko-naftni zbornik, 38(5), 79-86. https://doi.org/10.17794/rgn.2023.5.7

Kim, S. H.(1996). Model testing and analysis of interactions between tunnels in clay (Doctoral dissertation, University of Oxford).

Krishna, G., & Maji, V. B. (2023). Tunnelling induced ground settlement considering soil variability. International Journal of Mining and Geo-Engineering, 57(1), 59-64. DOI: 10.22059/ijmge.2022.328759.594922

Lee, I. M., & Nam, S. W. (2001). The study of seepage forces acting on the tunnel lining and tunnel face in shallow tunnels. Tunnelling and Underground Space Technology, 16(1), 31-40. https://doi.org/10.1016/S0886-7798(01)00028-1

Loganathan, N., & Poulos, H. G. (1998). Analytical prediction for tunneling-induced ground movements in clays. Journal of Geotechnical and geoenvironmental engineering, 124(9), 846-856. https://doi.org/10.1061/(ASCE)1090-0241(1998)124:9(846)

Mair, R. J., Taylor, R. N., & Bracegirdle, A. (1993). Subsurface settlement profiles above tunnels in clays. Geotechnique, 43(2), 315-320. https://doi.org/10.1680/geot.1993.43.2.315

Najjar, Y., & Zaman, M. (1993). Surface subsidence prediction by nonlinear finite-element analysis. Journal of geotechnical engineering, 119(11), 1790-1804.

Oteo, C., & Moya, J. F. (1979). Evaluación de parámetros del suelo de Madrid con relación a la construcción de túneles. In Proceedings of the 7th European Conference on Soil Mechanics and Foundation Engineering, Brighton (Vol. 3, No. 13, pp. 239-247).

Peck, B. B. (1969). Deep excavation and tunnelling in soft ground, State of the art volume. In 7th ICSMFE (Vol. 4, pp. 225-290).

Rostami, A. H. (2017). Estimation of settlements induced in tunneling with TBM in Urban Environments. Case study: Isfahan Subway Line 1 (Doctoral dissertation, Ph. D. Unpublished, Ph. D. Thesis in Mining Engineering).

Sagaseta, C. (1987). Analysis of undrained soil deformation due to ground loss. Geotechnique, 37(3), 301-320. DOI: 10.1680/geot.1987.37.3.301

Sakcali, A., & Yavuz, H. (2019). Estimation of radial deformations around circular tunnels in weak rock masses through numerical modelling. International Journal of Rock Mechanics and Mining Sciences, 123, 104092, 1-14. https://doi.org/10.1016/j.ijrmms.2019.104092

Sakcali, A., & Yavuz, H. (2022). Prediction of the longitudinal ground pressure-acting roof of the shield during single-shield TBM excavation in weak rock masses. Bulletin of Engineering Geology and the Environment, 81(11), 477, 1-19. https://doi.org/10.1007/s10064-022-02958-8

Schmidt B (1969) A method of estimating surface settlement above tunnels constructed in soft ground. Can Geotech J 20:11–22. DOI:10.1139/t83-002

Selby, A. R. (1999). Tunnelling in soils–ground movements, and damage to buildings in Workington, UK. Geotechnical & Geological Engineering, 17, 351-371. https://doi.org/10.1023/A:1008985814841

Unlu, T., & Gercek, H. (2003). Effect of Poisson's ratio on the normalized radial displacements occurring around the face of a circular tunnel. Tunnelling and Underground Space Technology, 18, 547-553. https://doi.org/10.1016/S0886-7798(03)00086-5

Vahdati, P., Levasseur, S., Mattsson, H., & Knutsson, S. (2014). Inverse hardening soil parameter identification of an earth and rockfill dam by genetic algorithm optimiza-

tion. The Electronic journal of geotechnical engineering, 19(N), 3327-3349.

Verruijt, A., & Booker, J. R. (1998). Surface settlements due to deformation of a tunnel in an elastic half plane. Geotechnique, 48(5), 709-713.

Vlachopoulos, N., & Diederichs, M. S. (2009). Improved displacement profiles for convergence confinement analysis of deep tunnels. Rock Mechanics and Rock Engineering, 42, 131-146. https://doi.org/10.1007/s00603-009-0176-4

Wang, J., Zhou, P., Song, Z., Li, S., & Zhang, Q. (2022). A new calculation method for tunneling-caused stratum settlement. KSCE Journal of Civil Engineering, 26(6), 2624-2640. https://doi.org/10.1007/s12205-022-1258-z

Wang, Z. W., Sampaco, K. L., Fischer, G. R., Kucker, M. S., Godlewski, P. M., & Robinson, R. A. (2000). Models for predicting surface settlements due to soft ground tunneling. In North American Tunneling 2000American Underground Construction Association.

Zhao, C., Lavasan, A. A., Barciaga, T., Kämper, C., Mark, P., & Schanz, T. (2017). Prediction of tunnel lining forces and deformations using analytical and numerical solutions. Tunnelling and Underground Space Technology, 64, 164-176. https://doi.org/10.1016/j.tust.2017.01.015

SAŽETAK

Predviđanje slijeganja dvocijevnih tunela korištenjem genetskih algoritama – studija slučaja: Isfahan, Iran

Povećanjem urbanizacije i rasta stanovništva značajno se povećala potražnja za tunelima podzemne željeznice. Ti se tuneli često grade na malim dubinama i u neposrednoj blizini urbane infrastrukture. U takvim prilikama ključno je zaštititi zgrade i druge građevine od potencijalne štete uzrokovane iskopavanjem tunela. Stoga je proučavanje pomaka tla i površinskih slijeganja u blizini tunela ključno za sigurnost površinskih građevina. Na temelju geotehničkih karakteristika istraživanog područja i podataka prikupljenih tijekom iskopavanja dvocijevnih tunela s strojem za bušenje tunela (Tunnel Boring Machine TBM) u ovom istraživanju razvijena je empirijska metoda za procjenu slijeganja, maksimalnog slijeganja i točaka infleksije. Za derivaciju tih parametara korištene su Boltzmannove i Gaussove funkcije. Nakon toga provedena je analiza osjetljivosti pomoću 3D programa Plaxis za poprečni presjek Si-o-se-pol područja uzduž tri različita tipa tla. Zatim je predložena numerička veza za procjenjivanje maksimalnog slijeganja tla korištenjem genetskog algoritma. Rezultati su pokazali snažnu usklađenost između empirijskih podataka i numeričkog pristupa primijenjenog u ovoj studiji. Zbog svega toga, ova saznanja omogućuju točnije predviđanje slijeganja tla za liniju podzemne željeznice Isfahan 2, koja je trenutno u fazi iskapanja.

Ključne riječi:
Slijeganje, maksimalno slijeganje, točka infleksije, empirijska formula, numerička formula

Author's contribution

Amirhossein Rostami (PhD, Associate Professor) provided and wrote the paper. **Hamid Chakeri** (PhD, Associate Professor) proposed the idea and guided the research. **Kurosh Shahriar** (PhD, Professor) proposed the idea and guided the research. **Masoud Cheraghi Seifabad** (PhD, Associate Professor) proposed the idea and guided the research.
All authors have read and agreed to the published version of the manuscript.